JOURNAL OF STRUCTURAL BIOLOGY **120,** 237–244 (1997)
ARTICLE NO. SB973914

Practical Image Restoration of Thick Biological Specimens Using Multiple Focus Levels in Transmission Electron Microscopy

Karen F. Han,[1] John W. Sedat, and David A. Agard

Graduate Group in Biophysics, Department of Biochemistry and Biophysics, Howard Hughes Medical Institute, University of California Medical School, San Francisco, California 94143-0448

Received September 9, 1997

Three-dimensional electron tomographic studies of thick specimens such as cellular organelles or supramolecular structures require accurate interpretations of transmission electron micrograph intensities. In addition to microscope lens aberrations, thick specimen imaging is complicated by additional distortions resulting from multiple elastic and inelastic scattering. Extensive analysis of the mechanism of image formation using electron energy-loss spectroscopy and imaging as well as exit wavefront reconstruction demonstrated that multiple scattering does not contribute to the coherent component of the exit wave (Han *et al.*, 1996, 1995). Although exit wavefront restored images showed enhanced contrast and resolution, that technique, which requires the collection of more than 30 images at different focus levels, is not practical for routine data collection in 3D electron tomography, where usually over 100 projection views are required for each reconstruction. Using a 0.7-μm-thick specimen imaged at 200 keV, the accuracy of reconstructions using small numbers of defocused images and a simple linear filter (Schiske, 1968) was assessed by comparison to the complete exit wave restoration. We demonstrate that only four optimal focus levels are required to effectively restore the coherent component (deviation 5.1%). By contrast, the optimal single image (zero defocus) shows a 25.5% deviation to the exit wave restoration. Two pairs of under- and over-defocus images should be taken: one pair at quite high defocus (>10 μm) to differentiate the coherent (single elastic scattering) from the incoherent (multiple elastic and inelastic scattering) components, and the second pair to optimize information content at the highest desired resolution (e.g., 5 μm for (2.5 nm)$^{-1}$ resolution). We also propose a new interpretation of the restored amplitude and phase components where the specimen mass-density is proportional to the logarithm of the amplitude component and linearly related to the phase component. This approach should greatly facilitate the collection of high resolution tomographic data from thick samples.

Key Words: **transmission electron microscopy; image restoration; thick specimens; electron tomography; through focus series.**

INTRODUCTION

High resolution three-dimensional (3D) analyses of cellular organelles and nuclear structures is most appropriately studied using transmission electron microscopic tomography of thick sections (Belmont *et al.*, 1987; Frank *et al.*, 1992; Fung *et al.*, 1994; Horowitz *et al.*, 1994; Ladinsky *et al.*, 1994; Moritz *et al.*, 1995). To accurately compute the three-dimensional reconstructions from a set of tilted images and for quantitative analyses, it is essential to properly relate the image intensities to the projected specimen mass densities. This relies on an accurate understanding of the image formation mechanism of these specimens in the transmission electron microscope (TEM). The images taken in the TEM are not always a direct representation of the specimen mass density. There are two sources of aberration that affect image formation: electron–specimen interactions and microscope lens aberrations. The difference between imaging of thick and thin specimens is at the level of electron–specimen interactions. For thin specimens, image formation is dominated by singly elastically scattered electrons, whereas for thick specimens, multiple elastic and multiple inelastic scattering contribute the majority of the electrons. In a detailed analysis of thick specimen image formation (Han *et al.*, 1996), we demonstrated previously that exit wavefront reconstruction can exclude most of the multiple scattering and correct for lens aberrations. As exit wavefront reconstruction requires many (often over 30) through focus images (Coene *et al.*, 1992; van Dyck *et al.*, 1990), it is

[1] Current address: Box 182, Northwestern University Medical School, Chicago, IL 60611.

1047-8477/97 $25.00

impractical for routine image restoration—particularly in the application to tomographic reconstruction, where a complete tilt data set requires over 100 projection images. It is therefore important to develop a more practical restoration approach that uses fewer focus levels yet can still exclude most of the multiple scattering component and also correct for the lens contrast transfer function.

In this paper we present a quantitative analysis of the application of the Schiske formalism to the imaging of thick biological specimens. We use a complete exit wave reconstruction based on 40 images as a standard for comparison. In addition, based on our experiments on the mechanism of image formation for thick sections, we propose a new way to combine the amplitude and phase contrast components to generate the restored image. This approach better accounts for the contribution of multiple scattering at low resolution.

MATERIALS AND METHODS

Thick biological specimens. The specimens used in the experiments described here were the same as were used in the previous paper (Han *et al.*, 1996). They are isolated centrosomes from Drosophila embryos embedded in epon and stained with uranyl-acetate and lead-citrate (Moritz *et al.*, 1995). The diameter of the microtubules, which are 22 nm, serve as an internal standard. Specimens were cut to 0.7-μm thickness.

Microscopy and through focus series. The energy-filtered images were recorded with a Gatan Imaging Filter, Model GIF100 (Gubbens *et al.*, 1993; Krivanek *et al.*, 1992) mounted on a Philips CM200. All TEM images were recorded at a calibrated magnification of 40 000 times at the CCD. The images were binned twice in the camera hardware resulting in an effective pixel size projected back to the specimen of 1.20 nm. A 10-μm objective aperture was used for all the experiments presented. The energy-window used for energy loss-filtered imaging was 10 eV, the energy dispersion used for recording the energy-loss spectra was 0.5 eV per CCD pixel.

Through focus series consisting of 41 images were recorded from 18.1 μm under focus to 18.1 μm over focus with a focus step size of 0.905 μm. To minimize specimen alterations and shrinkage (Braunfeld *et al.*, 1994) during data collection, the specimens were stabilized by preirradiating with approximately 1000 e^-/nm^2. The individual images were aligned prior to the exit surface wave front reconstruction using fiducial gold markers and cross-correlation (Koster *et al.*, 1992). Image processing and visualization were done on a DEC VAX-9000 and a Silicon Graphics Iris workstation using Priism, the image visualization software developed in our laboratory (Chen *et al.*, 1994).

THEORY

Many authors have presented approaches for image restoration (Coene *et al.*, 1992; Hawkes, 1980; Kirkland, 1982; Saxton, 1978; Scherzer, 1949; Schiske, 1968, 1973). Many such restorations are based on the assumption that the specimen is relatively thin and is a weak phase object. Typically, others have been interested in recovering very high resolutions ((~0.5–0.1 nm)$^{-1}$ range) where the contrast transfer function (CTF) is highly oscillatory. In such cases, recovery is particularly important because contrast inversions cause the image intensities to vary dramatically, making interpretation extremely difficult. In the study of thick biological specimens, we are interested in recovering a large range of relatively low resolutions, from (15 nm)$^{-1}$ to (3 nm)$^{-1}$. Here it is very difficult to recover the image wave due to the large fraction of multiple inelastic scattering contributing mostly in this resolution range. Since the CTF is varying slowly at low resolutions, it is also very difficult to uniquely restore the exit wave unless large values of defocus are used. For thick specimens, only the coherent component (single elastic scattering) exhibits the expected behavior of wave propagation through focus (Han *et al.*, 1995). Linear exit wave restoration techniques can be used to extract that coherent component which will exhibit an enhanced contrast throughout a large resolution range. Following the restoration, real and imaginary components of the exit wave must be properly related to the specimen mass density, using the experimental results that address the nature of image formation for thick specimens.

Van Dyck and coworkers have shown that the specimen exit wavefront can be restored by extracting the information which map on to a parabola in the three-dimensional Fourier transform of a through focus series (>30 images) (Coene *et al.*, 1992; van Dyck *et al.*, 1990):

$$\begin{aligned}\hat{\mathbf{I}}(\mathbf{k}, \zeta) = {} & |C|^2\delta(\mathbf{k}) + C^*\hat{\psi}(\mathbf{k})\delta(\zeta - \lambda|\mathbf{k}|^2/2) \\ & + C\hat{\psi}^*(-\mathbf{k})\delta(\zeta + \lambda|\mathbf{k}|^2/2) \\ & + \int_{\mathbf{k}\neq 0,(k-k')\neq 0} \hat{\psi}^*(\mathbf{k})\hat{\psi}(\mathbf{k} - \mathbf{k}') \\ & \cdot \delta[\zeta[(\mathbf{k} - \mathbf{k}')^2 - \kappa^2]/2]d\mathbf{k}'\end{aligned} \tag{1}$$

where $\mathbf{k}$ and ζ are reciprocal axes for x, y, and z, respectively; δ is the Dirac delta function; λ is the electron wavelength; $\hat{\mathbf{I}}(\mathbf{k}, \zeta)$ is the 3D Fourier transform of the image, and $\hat{\psi}$ is the specimen exit surface wavefront in Fourier space. By back transforming along the parabola, the exit wavefront can be recovered as follows:

$$\begin{aligned}\hat{\psi}_e = {} & \exp(i\pi C_s\lambda^3\mathbf{k}^4)\frac{1}{N} \\ & \cdot \sum_{\Delta f_n=1}^{N} \hat{\mathbf{I}}(\mathbf{k}, \Delta f_n)\exp(-i\pi\lambda\mathbf{k}^2\Delta f_n)\end{aligned} \tag{2}$$

Although Eq. (2) is essentially the same as the simplified Schiske restoration filter (Eq. 3, see below) (Saxton 1994; Schiske 1968), the mapping of

electrons in the 3D power spectra is an informative technique to select the appropriate focus levels to restore the resolution range of interest. For thick biological specimens, it was shown that a large central (incoherent) component can be isolated from the parabolic (coherent) component. The central component is contributed largely by inelastic multiply scattered electrons (Han *et al.*, 1996, 1995). The derivation by van Dyck *et al.* (1990) suggested that a large evenly spaced through focus series (>30 images) is optimal for restoration, which is, however, impractical in routine 3D tomography. The advantage of restoration using a wide range of focus levels is, in addition to the reduction of statistical noise by $\sqrt{N}$ (where N is the total number of images used in the restoration), a better separation between the parabolic (coherent) and incoherent components by reducing the width of the parabola in ζ (proportional to sinc (ζ), ζ is the full range of focus levels). Although it is not required to use an evenly spaced through focus series for restoration using Eq. (2), it is more desirable as it facilitates the use of FFTs to speed the calculations.

Although it is difficult to exclude multiple scattering by theoretical derivation, we can utilize the empirical results described above to select optimal focus levels and minimize the contribution of the multiple scattering component. From the 3D power spectrum of the through focus series, at low ζs (or high defoci), the coherent (parabola) component maps to the lowest resolutions of interest that are still distinguishable from the incoherent (central) component (Han *et al.*, 1996). Although at high levels of defocus there is very little high resolution contribution, the multiple scattering degradation to the low resolution coherent portion of the image is greatly reduced. This is particularly important if one is interested in restoring the intermediate to low resolution ranges. To restore the high resolution components with minimal background, focus levels should be chosen at the highest defocus which contributes to the coherent (parabola) component at the expected resolution range (given by $\Delta f = 2/\lambda\mathbf{k}^2$). If restoration is performed with more defoci, the levels should be chosen such that the coherent components maximally span the resolution range of interest in the 3D power spectrum.

Using electron energy-loss spectroscopic imaging (ESI), as mentioned above, we showed that only single elastically scattered electrons contribute to the behavior of Eq. (1) (Han *et al.*, 1995). By restoring this component through the resolution range of interest, the restored exit wave can then be properly related to projected specimen mass density. Schiske and other authors have optimized the statistics of

TABLE I

Trial	%*D*	Defocus levels used in the restoration (μm)
(1) 8 focus levels (A)	3.77	±18.10, ±9.05, ±5.43, ±3.62
(2) 6 focus levels (A)	3.99	±18.10, ±5.43, ±3.62
(3) 6 focus levels (B)	5.09	18.10, 5.43, 3.62, −2.72, −4.53, −9.05
(4) 6 focus levels (C)	8.05	±12.11, ±7.03, ±5.43
(5) 4 focus levels (A)	5.17	±18.10, ±5.43
(6) 4 focus levels (B)	8.01	18.10, 5.43, −9.05, −3.62
(7) 4 focus levels (C)	9.05	±12.11, ±7.03
(8) 4 focus levels (D)	12.14	±8.57, ±5.43
(9) 2 focus levels (B)	11.22	5.43, −4.53
(10) 2 focus levels (A)	15.85	18.10, −17.19
(11) in focus data	25.47	
(12) 905 nm under-focused data	29.66	
(13) 3.63 μm under-focused data	31.44	
(14) 5.43 μm under-focused data	32.97	
(15) 18.1 μm under-focused data	36.11	

Note. %*D* difference with respect to the full exit wavefront restoration (see text) is used to compare the restorations and raw data. The first column lists the trials referred to in the text; second column, the %*D*s; third column, the focus levels used in the restoration.

the restoration (Hawkes, 1980; Saxton, 1978; Schiske, 1968, 1973):

$$\hat{\psi}_e(\mathbf{k}) = \sum_{\Delta f_n=1}^{N} \hat{\mathrm{I}}(\mathbf{k}, \Delta f_n) \cdot r(\mathbf{k}, \Delta f_n)$$

$$r(\mathbf{k}, \Delta f_n) = \exp\left[i\chi(\Delta f_n, \mathbf{k})\right] \cdot \frac{\left\{N - \sum_{\Delta f_n=1}^{N} \exp\left[2i[\chi(\Delta f_m, \mathbf{k}) - \chi(\Delta f_n, \mathbf{k})]\right]\right\}}{\left\{N^2 - \left|\sum_{\Delta f_n=1}^{N} \exp\left[2i[\chi(\Delta f_m, \mathbf{k})]\right]\right|^2\right\}} \quad (3)$$

where $\hat{\psi}_e(\mathbf{k})$ is the exit wave in Fourier space, $\hat{\mathrm{I}}(\mathbf{k}, \Delta f_n)$ is the Fourier transform of the defocused image, and $\chi(\Delta f_n, \mathbf{k})$ is the well-known wave aberration function. In a through focus series with equal focus level increments as it was done by van Dyck and coworkers, Eq. (3) reduces to Eq. (2). Since our goal is to restore the exit wavefront using as few as four focus levels, Eq. (3) is the more appropriate.

Once an approximation to the exit wave has been recovered, it is necessary to properly relate the amplitude and phase components of the projected specimen mass density. Based on previous experiments aimed at understanding the mechanism of image formation for thick specimens, we have shown

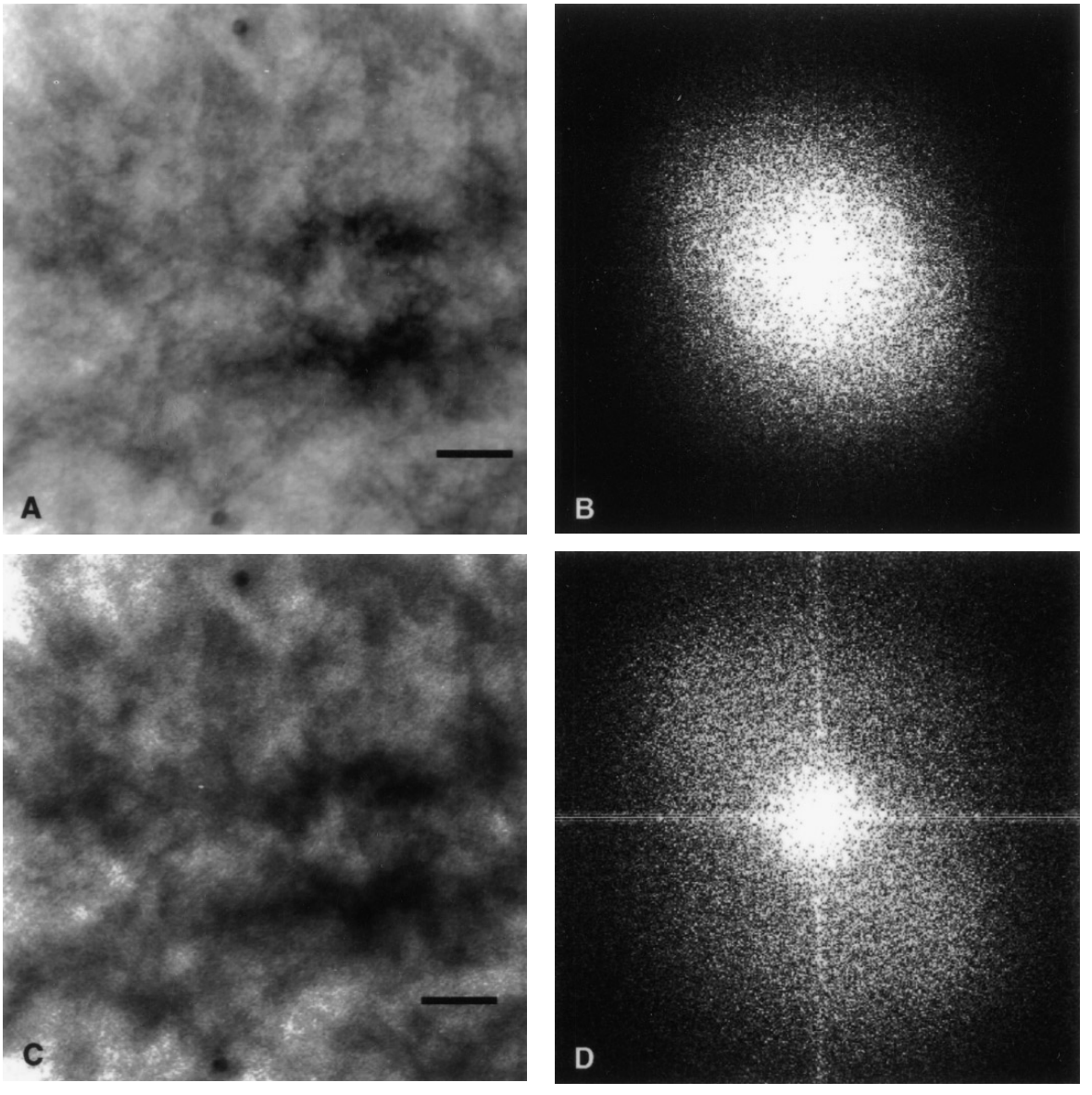

FIG. 1. Exit wavefront restoration (A) from 40 through focus images and its diffractogram (B); 905-nm defocused image (C) and its diffractogram (D). Scale bar, 100 nm, resolution limit is $(2.41\ \text{nm})^{-1}$.

that the relative contribution of elastic scattering component decreases with a logarithmic relationship to specimen thickness, whereas the multiple scattering component increases by the same relationship with thickness (Han *et al.,* 1995). The average image intensities in the same specimen area as a function of specimen tilt (hence thickness) also demonstrated a logarithmic relationship between intensity and thickness (data not shown). This is further illustrated by iterative 3D tomographic reconstructions, where the consistency between the reprojection of the model and the tomographic data is optimal when the image intensities between tilts are scaled by a logarithmic relationship. With respect to objective aperture-induced contrast, as previously demonstrated for thick specimens, the 10-μm aperture (effective resolution cut-off of $(0.3\ \text{nm})^{-1}$) efficiently blocks out a large proportion of the multiple scattering component without affecting specimen information at the resolution range of interest and does not contribute to the classical cosine component of the contrast transfer function (Han *et al.,* 1995). Indeed, Zeitler and Bahr have found this similar relationship, which they referred to as mass–thickness contrast. We thus interpret the restored amplitude component of the exit wave to arise directly from absorption by the thick specimen. As a consequence, the amplitude contrast component for

a thick specimen should have a logarithmic relationship to mass density. The phase component is interpreted to be directly related to specimen thickness and thus should follow a linear relationship. The sum of the phase component, $\phi(\mathbf{r})$, with the logarithm of the amplitude component, $A(\mathbf{r})$, is our estimate of the projected mass density distribution, $D(\mathbf{r})$, of the thick specimen:

$$D(\mathbf{r}) = \phi(\mathbf{r}) - \log [A(\mathbf{r})] \quad (4)$$

RESULTS

Comparison of the restoration using fewer focus levels with the Ewald sphere reconstruction. Since no absolute mass standard exists for thick biological specimens, it is difficult to assess whether the restored mass-distribution is "correct." Although the exact dimensions and mass distribution of the microtubules are known, the images are projections of often many overlapping microtubules, making the absolute assessment of mass density distribution difficult. Nonetheless, if we assume that the exit wavefront restoration using 40 focus levels gives the closest representation of the "true" mass density distribution, we can use it as a standard for comparison with different restoration techniques. As discussed under Theory, the Schiske filter was used to restore images from a through focus series (Eq. 3) (Schiske, 1968). To quantitatively compare the reconstructions while ignoring trivial differences due to different scales and background levels, the images were scaled by matching their contrast. The contrast image I' was calculated for each image as:

$$I'(x, y) = \frac{I(x, y) - I_{\text{ave}}}{I_{\text{ave}}}$$

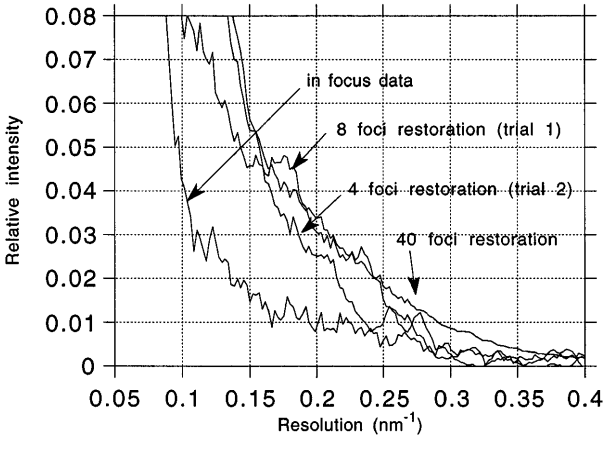

FIG. 2. Contrast and scale normalized power spectra comparing exit wavefront restored, 8-, 4-focus-level restored and in-focus data, demonstrating enhanced contrast.

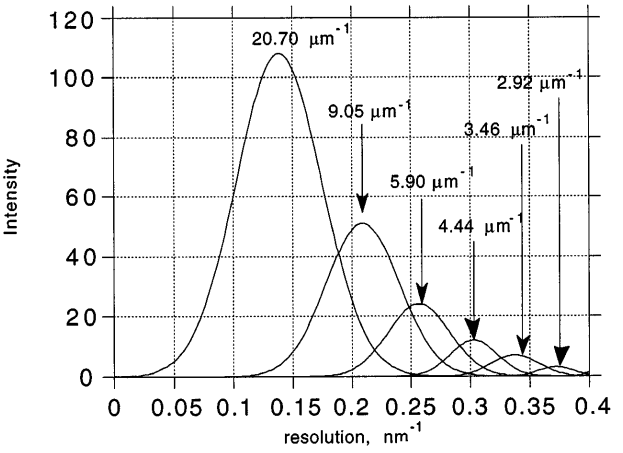

FIG. 3. Plot of the coherent component for each reciprocal defocus in the 3DFFT of the through focus series used to restore Fig. 1A.

and subsequently scaled to a common intensity range. Fractional deviation (%D) was used to assess the similarity between the restorations and the exit wavefront ($I'_{\text{ref}}(x, y)$):

$$\%D = \frac{100 \cdot \sum_{nx,ny} |I'(x, y) - I'_{\text{ref}}(x, y)|}{\sum_{nx,ny} |I'_{\text{ref}}(x, y)|}$$

In comparison to the complete reconstruction using 40 images, the restorations using fewer focus levels have reasonable fractional deviations (Table I). As expected, the more focus levels included in the restoration, the better the estimate of the exit wave (see Theory; Table I: trials 1, 2, and 5). The choice of focus levels strongly affects the restoration quality, and in the case of 4-focus level restoration, %D can range from 5 to 12% (Table I: trials 9–13). Indeed, any restoration is better than no restoration as evidenced by the high %Ds of the unrestored images. Of the unrestored images, the in-focus image remains closest to the 40-focus level restoration. This contrasts with the optimal Scherzer focus used in thin specimens, where phase contrast predominates. And as expected, the further out of focus a single image is (Table I, trials 12–15), the higher the %D due to the highly oscillatory behavior of the contrast transfer function.

Restoration using appropriately chosen four focus levels shows enhanced contrast. Figure 1 compares the in-focus image to the exit wavefront restored image for a 0.7-µm-thick specimen (see Methods) using Eq. (2) (see Theory). The exit wave reconstruction is used as a standard to compare with other restoration approaches using fewer focus levels. Figure 2 plots the power spectrum of the contrast

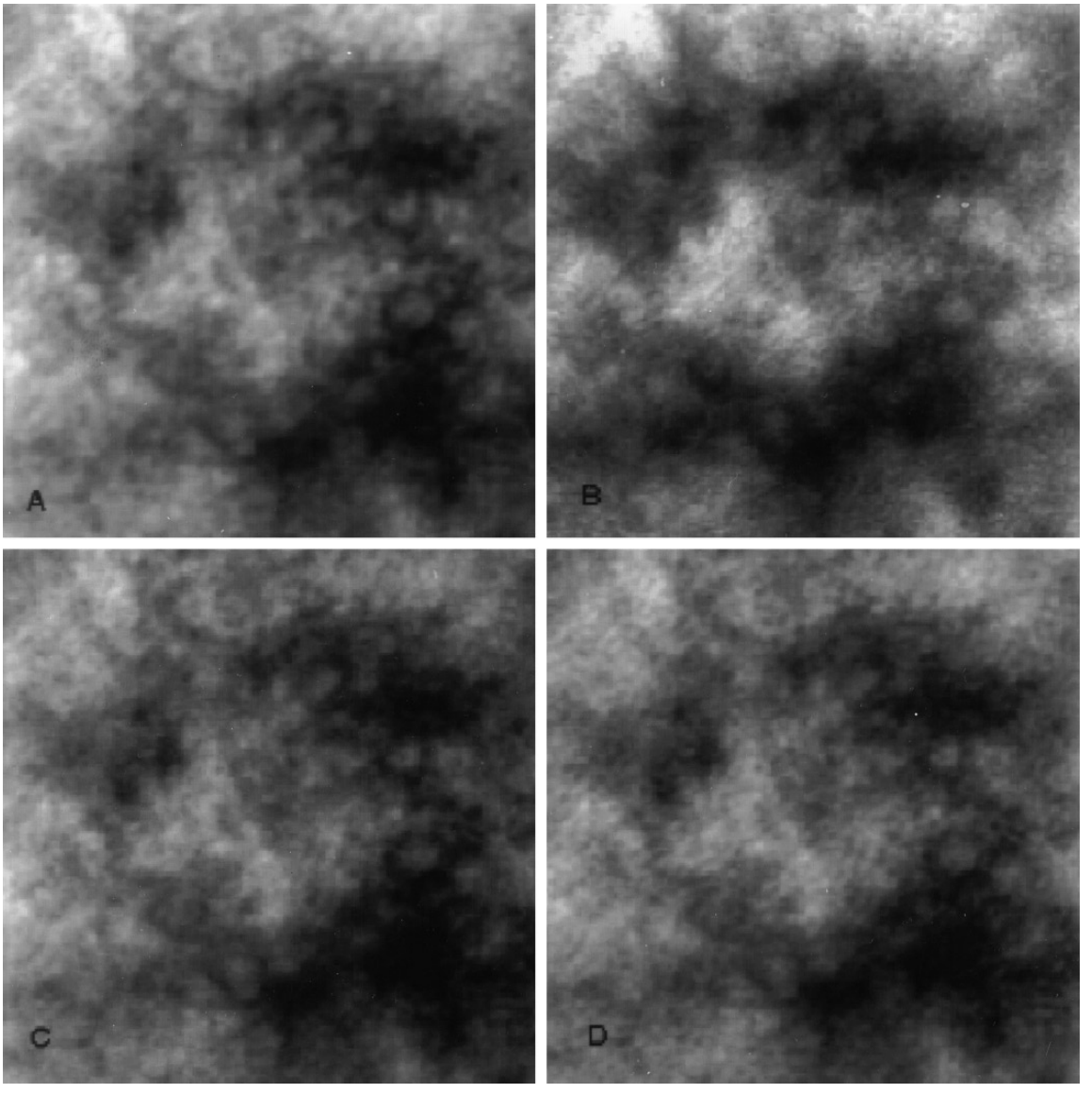

FIG. 4. Exit wave restoration (A), 905 defocused and restorations using 8 and 4 focus levels (C, D). Scale bar, 50 nm, resolution limit is $(2.41\ \text{nm})^{-1}$.

normalized images comparing the in-focus data, 8- and 4-focus-level restorations (Eq. 3), and the 40-focus-level Ewald sphere reconstruction (Eq. 2). Optimal focus levels are chosen as described under Theory, where the multiple scattering component is mostly excluded and the coherent component in the 3D FFT of the through focus series spans the resolution range of interest shown in Fig. 3. For restoration using 6 defoci, the range of focus levels is chosen to evenly span the resolution range between $(15\ \text{nm})^{-1}$ and $(3\ \text{nm})^{-1}$: ± 18.10, ± 5.43, and ± 3.62 μm defoci (trial 2, Table I). The %*D* for this restoration is only slightly higher than that restored using 8 defoci (trial 1, Table I), with a value of 3.99%. The optimal set of defoci for the restoration using only four focus levels is: ± 18.10 and ± 5.43 μm, with an %*D* value of 5.2%. Note that although it is not necessary to choose matching under- and over-foci for the restorations, doing so results in better discrimination between the amplitude and phase components (compare trials 2 and 3, 5 and 6 in Table I). Figure 4 shows the restored images using 8- and 4-focus levels with Eq. (3) to obtain an estimate of the projected specimen mass density. The restoration using 4-focus levels (Fig. 4D) has higher contrast compared to the in focus data (Fig. 4C), although it clearly has a much higher background (noise) component compared to the restorations using 8-focus levels or the exit wave obtained using 40 levels (Figs. 4A and 4B). In addition, the microtubule boundaries are much more

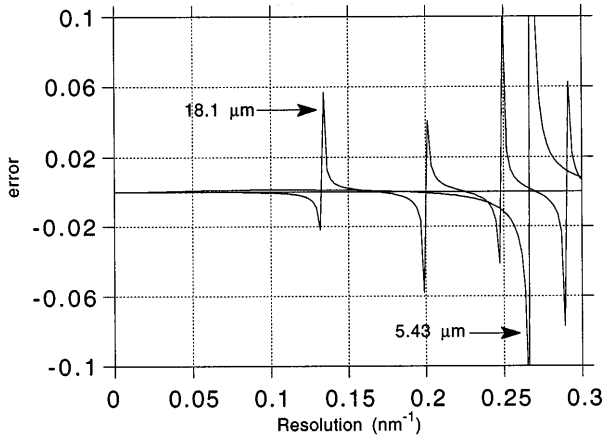

FIG. 5. Expected error of the contrast transfer function (CTF) as a function of resolution for focus levels used in the restoration described (Fig. 4) with a 10-nm focus level error.

clearly delineated in the restored images (Figs. 1A and 4A–4C) as compared to the unrestored (Fig. 4B).

The effect of error in focus level on the restorations. Figure 5 plots the expected error in the contrast transfer function (CTF) for a conserved estimate of the error in focus levels. Error at each focus level is determined by:

$$error = \frac{\left(\frac{d\mathrm{CTF}}{d(\Delta f)}\right)\epsilon_{\Delta f}}{\mathrm{CTF}} = \frac{\pi\lambda k^2(\beta \sin\chi + \cos\chi)\epsilon_{\Delta f}}{(\beta\cos\chi - \sin\chi) + \eta}$$

where β is the fraction of amplitude contrast (taken to be 0.15, empirically determined through curve-fits of diffractograms), $\epsilon_{\Delta f}$ is the estimated error in focus level determination (a conservative estimate is taken to be 10 nm), and η the estimated noise-to-signal ratio. The error in CTF is less than 2% for resolutions up to $(3\ \mathrm{nm})^{-1}$, except for regions where the CTF crosses zero (Fig. 5, spikes). Since the restoration is an over-determined problem, at resolutions where the CTF is crossing zero for one of the focus levels, the others are well-determined. Thus, the exit wave function is solvable within 2% for the entire range of the resolutions of interest.

DISCUSSION

An accurate three-dimensional tomographic reconstruction relies on the assumption that the recorded images accurately represent the projected specimen mass densities. While we have utilized a previously proposed restoration approach using only a few focus levels (Schiske, 1968), we demonstrated that it is important to choose focus levels that minimize the multiple scattering component in the restoration. The optimal focus levels for a four-level restoration requires one pair which are strongly defocused, thereby reducing the multiple scattering component at low resolution, and the other pair at levels at defoci where their contribution to the coherent component is the strongest at the expected (or goal) resolution. Our interpretation of the relationship between the exit wave and the specimen mass density differs from what has been traditionally assumed. Based on previous experiments, the mass density is better related to the amplitude component by a logarithmic relationship and phase through a linear relationship. In comparison with the full exit wave reconstruction, restorations using only a limited number of focal images can recover a good approximation to the "true" exit wavefront. We have demonstrated that the relative contrast through all resolutions is increased by removing aberrations from images of thick biological specimens. This enhanced contrast revealed substructures in these thick specimens that were otherwise not apparent in the uncorrected images. From these results, we demonstrate the importance of correcting for aberrations in electron micrographs to achieve an accurate interpretation of images for 3D reconstruction. The future incorporation of this modified restoration approach for thick specimens will improve the resolution extent of the 3D tomographic reconstructions.

The authors thank M. Braunfeld and M. Moritz for providing the centrosome specimens; A. Gubbens for assisting data collection and critical reading of this manuscript; A. Gubbens, W. Liu, M. Op de Beeck, M. Gustafsson for helpful discussions. K.F.H. is supported by the Howard Hughes Medical Institute Predoctoral Fellowship in the Biological Sciences. This work is supported by grants from the National Institutes of Health (GM 31627 for D.A.A.; GM25101 for J.W.S.) and by the Howard Hughes Medical Institute.

REFERENCES

Belmont, A. S., Sedat, J. W., and Agard, D. A. (1987) A three-dimensional approach to mitotic chromosome structure: Evidence for a complex hierarchical organization. *J. Cell Biol.* **105,** 77–92.

Chen, H., Clyborne, W., Sedat, J., and Agard, D. (1994) PRIISM: An integrated system for display and analysis of 3D microscope images. *SPIE: Biomed. Image Process. 3-D. Microsc.* **1660,** 784–790.

Coene, W., Janssen, G., Op de Beeck, M., and Van Dyck, D. (1992) Phase retrieval through focus variation for ultra-resolution in field-emission transmission electron microscopy. *Phys. Rev. Lett.* **69,** 3743–3746.

Frank, J., and Radermacher, M. (1992) 3-Dimensional reconstruction of single particles negatively stained or in vitreous ice. *Ultramicroscopy* **46,** 241–262.

Fung, J. C., Agard, D. A., and Sedat, J. W. (1994) Three-dimensional reconstruction of the synaptonemal complex from high-pressure frozen maize meiocytes using IVEM tomography. *Proc. 53rd Annu. Microsc. Soc. Am.* 14–15.

Gubbens, A., and Krivanek, O. (1993) Applications of a post-

column imaging filter in biology and material science. *Ultramicroscopy* **51,** 146–159.

Han, K. F., Gubbens, A. J., Koster, A., Braunfeld, M., Sedat, J. W., and Agard, D. A. (1993) Analysis of electron-specimen interactions of thick biological specimens in transmission electron microscopy at 200 keV. *52nd Annu. Microsc. Soc. Am*. 204–205.

Han, K. F., Gubbens, A. J., Sedat, J. W., and Agard, D. A. (1996) Optimal strategies for imaging thick biological specimens: Exit wavefront reconstruction and energy filtering. *J. Microsc.*, submitted.

Han, K. F., Sedat, J. W., and Agard, D. A. (1995) Mechanism of image formation for thick biological specimens: Exit wavefront reconstruction and electron energy-loss spectroscopic imaging. *J. Microsc.* **178(2),** 107–119.

Hawkes, P. W. (1980) Image processing based on the linear theory of image formation, *in* Computer Processing of Electron Microscope Images, Berlin, Pringer-Verlag.

Horowitz, R. A., Agard, D. A., Sedat, J. W., and Woodcock, C. L. (1994) The three-dimensional architecture of chromatin in situ: electron tomography reveals fibers composed of a continuously variable zig-zag nucleosomal ribbon. *J. Cell Biol.* **125,** 1–10.

Kirkland, E. J. (1982) Nonlinear high resolution image processing of convectional transmission electron micrographs. *Ultramicroscopy* **9,** 45–64.

Koster, A. J., Chen, H., Sedat, J. W., and Agard, D. A. (1992) Automated microscopy for electron tomography. *Ultramicroscopy* **46,** 207–227.

Krivanek, O. L., Gubbens, A. J., Dellby, N., and Meyer, C. E. (1992) Design and 1st applications of a post-column imaging filter. *Microsc. Microanal. Microstruct.* **3,** 187–199.

Ladinsky, M. S., Kremer, J. R., Furcinitti, P. S., McIntosh, J. R., and Howell, K. E. (1994) HVEM tomography of the trans-Golgi network: Structural insights and identification of a lace-like vesicle coat. *J. Cell Biol.* **127,** 29–38.

Moritz, M., Braunfeld, M., Fung, J., Alberts, B., Sedat, J., and Agard, D. (1995) Three-dimensional structural characterization of centrosomes from early drosophila embryos. *J. Cell Biol.* **130,** 1149–1159.

Saxton, W. (1994) What is the focus variation method—is it new—is it direct. *Ultramicroscopy* **55,** 171–181.

Saxton, W. O. (1978) Computer Techniques for Image Processing in Electron Microscopy. New York, Academic Press.

Scherzer, O. (1949) The Theoretical Resolution Limit of the Electron Microscope. *J. Appl. Phys.* **20,** 20–26.

Schiske, P. (1968) Zur Frage der Bildrekonstruktion durch Fokusreihen. 4th European Conference on Electron Microscopy, p. 145.

Schiske, P. (1973) Image processing using additional statistical information about the object, *in* Image Processing and Computer-aided Design in Electron Optics, Academic Press, London.

van Dyck, D., and Op de Beeck, M. (1990) New direct methods for phase and structure retrieval in HREM. *Proc. 12th Int. Congress for Electron Microsc.* 26–27.